A three-dimensional finite-element model of gluteus medius muscle incorporating inverse-dynamics-based optimization for simulation of non-uniform muscle contraction

Junyan Li[1*], Marco A. Marra[2], Nico Verdonschot[2,3], Yongtao Lu[4*]

Institute:

[1]School of Science and Technology, Middlesex University, London, UK

[2]Department of Biomechanical Engineering, University of Twente, The Netherlands

[3]Orthopaedic Research Laboratory, Radboud Institute for Health Sciences, Radboud University Medical Center, The Netherlands

[4]Department of Engineering Mechanics, Dalian University of Technology, Dalian, China

Key words: 3D finite element muscle model; non-uniform muscle contraction; gluteus medius; optimization of muscle contraction; musculoskeletal modelling

Corresponding author:

Junyan Li

ljyjerry@gmail.com

School of Science and Technology, Middlesex University, London, United Kingdom

Yongtao Lu

yongtaolu@dlut.edu.cn

Department of Engineering Mechanics, Dalian University of Technology, Dalian, China

Abstract

Non-uniform contraction exists in many skeletal muscles and plays an important role in the function of the musculoskeletal system. Particularly in the gluteus medius (GM) muscle, its three subdivisions appear activated differently while performing various motion tasks. However, the non-uniform contractile mechanism of GM is poorly understood. In this study, a three-dimensional finite element (FE) model of GM was developed. Non-uniform contraction patterns of the three subdivisions of GM during abduction, internal and external rotation were simulated through an inverse-dynamics-based optimization approach. A set of sensitivity studies were also undertaken to evaluate the influence of parameters including the cost function of optimization and dimension of GM subdivisions on the predicted non-uniform contraction and biomechanics of the muscle. Contraction across GM was found to be highly non-uniform during various motions. The whole GM was activated during abduction, whereas only the anterior and posterior subdivisions were primarily involved in internal and external rotation, respectively. The active contractile stress in a subdivision during abduction was increased if its proportion in GM was expanded. The cost functions of minimizing the sum of active contractile stresses squared/cubed provide similar qualitative predictions of the trend of results. This approach provides the methodological basis to enable simulation of non-uniform muscle contraction using 3D musculoskeletal models.

Words count from the Introduction through the Acknowledgments: 3600

1. Introduction

Muscles play an important role in the function of the musculoskeletal system. Dysfunction of muscles leads to aberrant postures, non-physiological loads on joints and ligaments and, eventually, the progression of musculoskeletal disorders [1, 2]. The gluteus medius (GM) muscle is the prime hip abductor. Dysfunction of GM has been implicated in impaired gait patterns, low back pain, patellofemoral pain syndrome and many other lower limb injuries [3, 4].

A muscle usually consists of a number of motor neurons. When a motor neuron is activated, the muscle fibres innervated by the motor neuron become stimulated and contract. The electro-mechanics behaviour of muscles is closed associated with the spatio-temporal pattern of muscles [5-7]. As a motor neuron can be activated individually, contraction in many skeletal muscles, i.e. the contractile activity indicated by active contractile forces/stresses, is non-uniform [8, 9]. Particularly in GM, there are three anatomically distinct subdivisions with potential for independent neural control, and as a result, the three subdivisions of GM appear activated differently while performing various motion tasks [8, 10]. The anterior and medial subdivisions that have fibres oriented more parallel to the femur would be better positioned to abduct the hip than the posterior portion. The tilt of fibres in the anterior and posterior subdivisions with respect to the frontal plane suggests their roles in hip internal and external rotation, respectively [10, 11].

There are a number of studies on non-uniform muscle contraction, mostly using electromyography (EMG) [8, 11-13] or FDG-PET (monitor fluorodeoxyglucose (FDG) uptake through positron emission tomography (PET)) [14]. However, the reliability of using EMG as an approach to measure biomechanics of muscles is questionable due to uncertainties in the acquisition and conversion of EMG signals into biomechanical response of muscles. Apart from the substantial artefacts introduced by cross-talk from neighbouring muscles or from adjacent subdivisions of the same muscle [15], the use of surface EMG is inappropriate for the whole GM because the posterior GM is completely covered by the gluteus maximus muscle [8]. On the other hand, intramuscular EMG or FDG-PET is invasive and would alter the normal function of muscles [16, 17]. Furthermore, previous experimental studies do not explain the cause-and-effect relationship between non-uniform muscle contraction and motion, the synergistic mechanism among muscle subdivisions, or the sensitivity of muscle activities to parameters such as the dimension and strength of a subdivision.

This information is important for planning surgical treatments and rehabilitation programmes to reduce pain and disability involved in musculoskeletal disorders [18], but remains poorly understood.

Computer models serve as an alternative approach with the potential to provide comprehensive biomechanical analyses of non-uniform muscle contraction. Most of the previous computer models that offer predictive muscle contraction are based on multibody dynamics musculoskeletal simulations with muscles assumed as one-dimensional (1D) line-segment models [19, 20]. Using these musculoskeletal models, muscle forces can be calculated based on non-invasively measured kinematics. However, 1D muscle models have limitations for simulations of non-uniform muscle contraction, because such models lack the ability to incorporate realistic three-dimensional (3D) muscle geometry and spatial fibre architecture within muscles, which would limit their modelling accuracy [21]. Furthermore, 1D models do not provide parameters such as stresses, strains and distribution of non-uniform contraction of a muscle. These parameters are important for systematic biomechanical evaluation of muscles.

Muscle models with realistic 3D geometry and detailed fibre architecture have been developed using finite element (FE) method [21-24]. However, in these previous 3D muscle models, muscle contractions were among the inputs rather than being calculated, because the redundancy issue, i.e. muscles outnumber equations of equilibrium requiring optimization to determine a unique solution of muscle contractions, was not addressed. This hampers the application of previous 3D models to study non-uniform muscle contraction. Furthermore, FE models of GM is not available yet. In a recent forward dynamics-based 3D FE musculoskeletal model [25], proportional-integral-derivative (PID) controllers were introduced to calculate muscle activations. Recently, we have developed an inverse dynamics-based FE musculoskeletal model with the ability to predict 3D muscle contractions based on kinematic data [26]. However, in these models, the contraction across each muscle was assumed to be uniform.

Therefore, the aim of this study was to develop a 3D FE model of the GM muscle incorporating inverse-dynamics-based optimization that was capable of simulating non-uniform contraction of the muscle during different motions. Additionally, a set of sensitivity studies were undertaken to evaluate the influence of parameters including the cost function of optimization and dimension of GM subdivisions on the predicted non-uniform contraction and biomechanics of the muscle.

2. Materials and Methods

In this study, subject-specific 3D geometric models reconstructed from magnetic-resonance-imaging (MRI) in the TLEM 2.0 database [27] including the GM muscle, femur and pelvis of the right lower extremity were adopted. Using a meshing software package (Hypermesh V2017, Altair, USA), the muscle and bones were represented with 4605 eight-noded hexahedral elements and 23743 four-noded tetrahedral elements, respectively (**Fig. 1a**). The mesh was dense enough to ensure the change in the peak tensile stress and active contractile stress was within 5% if the number of elements of the muscle was doubled.

Through the insertion/origin sites of the muscle/tendon tissue that are based on the anatomical information provided in TLEM 2.0 [27], the muscle/tendon tissue was rigidly attached to the bones. As deformation of joints and bones was not the subject of interest in this study and was minimal comparing to the deformation of muscles [28], the hip was assumed as a three degrees-of-freedom ball-and-socket joint and bones as rigid in order to enhance computational efficiency.

Both active and passive properties of the muscles were considered. Incompressible transversely isotropic Mooney-Rivlin material [29] incorporating fibres was adopted to represent the tendons and passive properties of the muscles. The fibre orientation within GM (**Fig. 1b**) and the regions of tendon and muscle tissues (**Fig. 2**) were identified using anatomical knowledge [10, 30]. The strain energy W of this constitutive model was given in [31]:

$$W = F_1(I_1, I_2) + F_2(\lambda) + \frac{K}{2}[\ln(J)]^2 \tag{1}$$

where, the function F_1 represents the material response of the isotropic ground substance matrix in the form of Mooney-Rivlin material as described in Eq. (2); F_2 contribution from the fibres as illustrated in Eq. (3); J volume ratio; K a bulk modulus-like penalty parameter.

$$F_1 = \frac{C_1}{2}(I_1 - 3) + \frac{C_2}{2}(I_2 - 3) \tag{2}$$

where, C_1 and C_2 are the Mooney-Rivlin material coefficients; I_1 and I_2 first and second strain invariants of the deviatoric Cauchy–Green tensor C.

$$\lambda\frac{\partial F_2(\lambda)}{\partial\lambda} = \begin{cases} 0 & \lambda \le 1 \\ C_3\left(e^{C_4(\lambda-1)} - 1\right) & 1 < \lambda < \lambda_m \\ C_5\lambda + C_6 & \lambda \ge \lambda_m \end{cases} \tag{3}$$

where, λ is the deviatoric part of the stretch along the fibre direction; λ_m stretch at which the fibres are straightened; C_3 scales the exponential stresses; C_4 rate of uncrimping of the fibres; C_5 modulus of the straightened fibres; C_6 determined to ensure continuous stress at λ_m. λ is usually bigger than zero as it reflects fibre stretch; $\lambda < 1$ describes the material in compression; $\lambda > 1$ describes the material in tension. Active contraction along the fibres was incorporated into the muscle material model (**Fig. 1b**), with the total stress in the solid mixture ($\boldsymbol{\sigma}$) as the sum of the solid stress due to strain ($\boldsymbol{\sigma}^{\mathbf{s}}$) and the active contractile stress ($\boldsymbol{\sigma}^{\mathbf{a}}$):

$$\boldsymbol{\sigma} = \boldsymbol{\sigma}^{\mathbf{s}} + \boldsymbol{\sigma}^{\mathbf{a}} \tag{4}$$

Values of the parameters in the constitutive model are shown in **Table 1**. Three subdivisions were defined in the GM model, with independent active contractile stress in each of the portions (**Fig. 2**). Uniform contraction was assumed in each subdivision. The three subdivisions were of similar dimensions in the original model (**Fig. 2a**). To assess the effect of the dimension of subdivisions on the model predictions, three other models were created in which the cross-sectional area of one of the three GM subdivisions was approximately 1.5 times larger than the other two portions (**Fig. 2b, c** and **d**). This choice of proportion and variation is based on anatomical observations [10, 30].

The pelvis was immobilized in all degrees-of-freedom. Motions that GM contributes to including abduction, internal rotation and external rotation [11] were applied to the hip joint separately (through rotating the femur), starting from 0 degrees to 20 degrees and ramped over 0.5 s. Flexion, extension and adduction were not investigated, because GM plays a minor role in these motions. Except for the insertion/origin sites of the muscle/tendon tissue connecting the bones, the GM muscle is not anatomically in contact with the bones. Therefore, contact between the muscle and bones was not defined in the model to enhance computation efficiency.

During each motion, there are three unknown active contractile stresses to be calculated versus one moment equilibrium equation which is along the axis of rotation of the hip joint. In order to solve this redundancy issue, optimization is needed to determine a unique solution of active contractile stresses in the subdivisions. Therefore, an inverse-dynamics-based optimization approached was developed. Based on the muscle active contractile stresses and the corresponding joint moments in the FE model, active contractile stresses in the subdivisions of the FE GM model were optimized until 1) the cost function was minimized and 2) constant resisting moments of 5.0 N×m, 0.2 N×m, and 0.5 N×m along the axis of rotation of the hip joint were generated by GM during abduction, internal rotation and external rotation, respectively (e.g. adduction moment generated during abduction). These moments would ensure a proper level of activation for GM (this is equivalent to applying torques to the joint for the muscle to balance). The two cost functions that have been widely used in recent musculoskeletal models of the lower extremity including minimizing the sum of active contractile stresses squared (i.e. $\sum_{i=1}^{n}({\sigma^{\mathrm{a}}}_{i})^{2}$) [32] and minimizing the sum of active contractile stresses cubed (i.e. $\sum_{i=1}^{n}({\sigma^{a}}_{i})^{3}$) [33] were simulated to evaluate the sensitivity of the model to the cost functions. Another cost function that minimizes the maximum active contractile stress (i.e. $\min(\max(\sigma^{a}))$) was also assessed [34]. Results of non-uniform muscle contractions under different cost functions were compared to a GM model with uniform muscle contraction across the whole muscle. Notably, the system with uniform GM contraction is not redundant and thus optimization is not needed. Optimization and analyses were conducted at 0 degrees, 5 degrees, 15 degrees and 20 degrees for each motion. The muscle lengths and moment arms were recalculated at each optimization step.

FE modelling was performed in the open-source implicit FE solver FEBio (V2.6.4; http://febio.org/febio). To enhance computational efficiency, the FE model at each quasi-static time instance (e.g. at 0.5 s) in the optimization process was simulated based on the model at the previous time instance (i.e. at 0.4 s) in which the optimization criteria were achieved, rather than starting from the original state (i.e. at 0 s). Optimization and automation of data transfer between the FE modelling and optimization procedures were achieved in MATLAB (R2017a, Mathworks, MA). The "fmincon" optimization tool in MATLAB was adopted to solve the optimization problem. The simulations were performed on a Windows 10 computer with 64 GB of RAM and 32 Intel E5-2699 cores at 2.2 GHz. Active contractile stresses and tensile stresses (i.e. the first principal stress of $\boldsymbol{\sigma}$ in Eq (4)) of the GM muscle were analyzed.

3. Results

Distribution of tensile stresses across the GM model during different motions is shown in **Fig. 3**. Tensile stresses were concentrated around the tissue region connecting the femur, where the tissue has smaller cross-sectional area than in the rest of the GM. Tensile stresses in all the subdivisions were of similar levels during hip abduction. Among the three subdivisions, tensile stresses were markedly higher in the anterior subdivision and posterior subdivision during internal rotation and external rotation, respectively. For each motion, the maximum tensile stress was higher at 20 degrees rotation than in the original configuration.

As shown in **Fig. 4**, active contractile stresses increased with increasing rotation angle of all the motions, in particular during internal and external rotation. The whole GM were activated during abduction, while only the anterior subdivision displayed contraction during internal rotation. During external rotation, both the medial and posterior subdivisions were activated from 0 degrees to 5 degrees, while the medial subdivision became inactivated when the rotation exceeded 10 degrees.

During abduction, active contractile stresses in the anterior and medial subdivisions were similar and higher than the posterior portion.

The active contractile stresses were different under different cost functions during abduction, particularly in the posterior subdivision (**Fig. 5**). Results of the models with uniform contraction and with the cost function of minimizing the maximum active contractile stress were identical, but different from the other two models. Under the two cost functions of minimizing the sum of active contractile stresses squared/cubed, the active contractile stress increased with increasing abduction angle and was higher in the anterior and medial subdivisions than the posterior portion. A higher level of non-uniform contraction was observed under the cost function of minimizing the sum of active contractile stresses squared than minimizing the sum of active contractile stresses cubed. As shown in **Fig. 6**, there was also a difference in active contractile stresses among the models with subdivisions of different dimensions. The active contractile stress was higher in a larger subdivision during abduction than the same subdivision of the model with subdivisions of similar dimensions.

4. Discussion

In this study, non-uniform contraction of the GM muscle during different motions was simulated for the first time through a novel approach combining FE modelling and inverse-dynamics-based optimization. It was found that contraction in GM is highly non-uniform across its subdivisions during different motions. This is generally in agreement with previous EMG and FDG-PET studies [8, 11-14]. There was also a marked difference in the biomechanics of GM between the models with and without the consideration of non-uniform contraction. These findings demonstrate the important role of non-uniform muscle contraction while performing various motion tasks as well as the great need to consider non-uniform muscle contractions in musculoskeletal models.

Computer models have the advantage over experimental measurements in terms of elucidating the synergistic mechanism among muscles. In theory, every agonistic muscle in the musculoskeletal system should be activated to some extent under the cost function of minimizing the sum of active contractile stresses squared or cubed [35]. In this study, it was shown that all the GM subdivisions contribute to hip abduction, while only the anterior and posterior subdivisions are primarily activated during hip internal and external rotation, respectively. This would suggest that the anterior and posterior subdivisions act as agonists during abduction but as antagonists to each other during internal (anterior subdivision as the agonist) and external (posterior subdivision as the agonist) rotation. This is also reflected by the finding that contraction in the anterior (or posterior) subdivision increases with increasing internal (or external) rotation angle in order to balance the increased passive tension in the posterior (or anterior) portion. These results contradict a previous surface EMG measurement, where it was found that the anterior subdivision displayed higher activation than the posterior portion during both internal and external rotation [13], but are supported by the anatomical observation that the orientation of fibres in the anterior and posterior subdivisions would reflect their participation in internal and external rotation, respectively [10]. It was found that the collaborative pattern among GM subdivisions does not only depends on the type of motion, but is also subject to the level of external rotation. The medial subdivision took part in the initial external rotation but became an antagonist to external rotation above 10 degrees.

The proportion in the dimension of each subdivision in GM varies between individuals [10, 30]. Additionally, it is unclear whether the cost functions of optimization used in previous musculoskeletal models would provide contradictory results when applied to simulate non-uniform muscle contraction. The parametric study was therefore undertaken as a precursor to future model validation to identify the sensitivity of the model to these parameters. The findings of this study show that contraction patterns of GM are dependent on the dimension of its subdivisions. The level of contraction in a subdivision during abduction was increased if its proportion in GM was expanded, because of its ability of sharing a higher proportion of the hip adduction moment applied [35]. Compared to previous musculoskeletal models in which the GM was typically represented by three independent 1D line-segments [36], this study offers more systematic analyses of the distribution of activation and stresses across the 3D structure, and at the same time, accounting for the shear effect between the connecting subdivisions. In this study, only the results during abduction are shown to demonstrate the sensitivity of the model to the cost functions and the dimension of the muscle subdivisions. This is because that only the anterior and posterior subdivisions were primarily activated during internal and external rotation, respectively. As a results, various cost functions and dimensions of the muscle subdivisions provided similar predictions during internal and external rotation.

The two cost functions of optimization that have been widely used in previous musculoskeletal models of the lower extremity, i.e. minimizing the sum of active contractile stresses squared/cubed, were found to result in different levels of muscle contraction during abduction, but provide similar trends in the relationship between contraction and rotation angle and in the comparison of contractions between subdivisions. Further experimental measurements and validation studies are needed to determine the optimal cost function in future modelling of 3D muscles. Under both cost functions, the level of contraction increased with increasing abduction angle and was higher in the anterior and medial subdivisions than the posterior portion. This is consistent with the anatomical observation that the anterior and medial subdivisions have fibres oriented more parallel to the femur and thus would be better positioned to abduct the hip than the posterior portion [10]. Reliable experimental quantification of muscle co-contraction is needed to determine the optimal cost function. However, the non-uniform contraction pattern of GM during abduction cannot be predicted using the cost function of minimizing the maximum active contractile stress. It should be noted that co-contraction from antagonistic muscles or antagonistic muscle subdivisions is not considered in these cost functions of optimization. A higher level of contractions in all the subdivisions could be expected in a model considering co-contraction. Although co-contraction would offer similar qualitative predictions regarding the trend of results and the comparison between models, it will be considered in future studies once reliable experimental quantification of muscle co-contraction is available.

Obviously, there were a number of limitations in this study. First, the non-uniform contraction that could further exist in each GM subdivision would provide smoother distribution of stresses and strains across the muscle compared to the current model assuming uniform contraction in each subdivision. This aspect was not accounted for in the current model, since such studies are not available yet for comparison. Secondly, it was assumed that motor neurons mainly stimulate active stresses of muscles, so only active stresses were optimized in this study. However, passive stresses and strains would also play a role in the muscle recruitment pattern, which will be a future consideration. Additionally, the material properties of the muscle were adopted from the literature. Variation in material properties among individuals and muscles should be considered for future subject-specific studies. Constitutive models accounting for the effect of fibre stretches and velocity on the level of muscle activation and derived specifically for modelling of muscles (e.g. coupling of active and passive stresses) [37-39] will also be a consideration in future studies. Although the modelling and optimization procedures are based on a validated algorithm [26, 40], the GM model itself was not validated due to the challenge in experimental measurements of the biomechanical behaviour of GM. Future more reliable experimental measurements, perhaps through dynamic imaging [41, 42], would provide alternative data to validate the change in morphology of the muscle model due to contraction. In the current model, the other abductor and rotator muscles of the hip were not accounted for, since the purpose of this study was to evaluate the activity of GM performing various rotation tasks under constant moments. However, the surrounding tissues would have an effect on the biomechanical behaviour of the muscle [26]. Apart from the motions simulated in this study, other motions including flexion, extension and adduction were not investigated, because GM was found to play a minor role in these motions. The muscle model with non-uniform contraction developed in this study will be incorporated into a 3D FE musculoskeletal modelling framework we have developed recently [26] to enable more realistic musculoskeletal modelling and simulations of a wider range of activities such as gait in future work. However, these assumptions do not affect the qualitative predictions of this study, i.e. biomechanical differences found between models during different motions and with different cost functions and dimensions of subdivisions.

In conclusion, a 3D FE model of the GM muscle incorporating inverse-dynamics-based optimization was developed to simulate non-uniform contraction of the muscle. Contraction across GM was found to be highly non-uniform during various motions. The whole GM was activated during abduction, whereas only the anterior and posterior subdivisions were primarily involved in internal and external rotation, respectively. The proportion in the dimension of each GM subdivision had an effect on the predictions and therefore may be important to consider for subject-specific modelling of non-uniform muscle contraction. The cost functions of optimization that have been widely used in previous musculoskeletal models of the lower extremity, i.e. minimizing the sum of active contractile stresses squared/cubed, provide similar qualitative predictions of muscle activity. This computational approach has the potential to aid in understanding the mechanisms of muscle function and the pathology of musculoskeletal impairments. Future attempts will also be made to simulate the electro-mechanics behaviour of muscles using the modelling and optimization framework.

Acknowledgements

This research was supported by the Newton Fund of the British Council 2017-RLWK9-10075 and the Open Fund from the China State Key Laboratory of Structural Analysis for Industrial Equipment (GZ19108). The author appreciates the efforts of the developers of FEBio.

References

1. Brandt, M., et al., *Participatory intervention with objectively measured physical risk factors for musculoskeletal disorders in the construction industry: study protocol for a cluster randomized controlled trial.* BMC Musculoskeletal Disorders, 2015. **16**(1): p. 302.
2. Golabchi, F.N., et al., *Assessing aberrant muscle activity patterns via the analysis of surface EMG data collected during a functional evaluation.* BMC musculoskeletal disorders, 2019. **20**(1): p. 13-13.
3. Niemuth, P.E., et al., *Hip muscle weakness and overuse injuries in recreational runners.* Clinical Journal of Sport Medicine, 2005. **15**(1): p. 14-21.
4. Nakagawa, T.H., et al., *Trunk, pelvis, hip, and knee kinematics, hip strength, and gluteal muscle activation during a single-leg squat in males and females with and without patellofemoral pain syndrome.* Journal of Orthopaedic & Sports Physical Therapy, 2012. **42**(6): p. 491-501.
5. Gizzi, A., et al., *Theoretical and Numerical Modeling of Nonlinear Electromechanics with applications to Biological Active Media.* Communications in Computational Physics, 2014. **17**(1): p. 93-126.
6. Klotz, T., et al., *Modelling the electrical activity of skeletal muscle tissue using a multi-domain approach.* Biomechanics and Modeling in Mechanobiology, 2020. **19**(1): p. 335-349.
7. Loppini, A., et al., *Competing Mechanisms of Stress-Assisted Diffusivity and Stretch-Activated Currents in Cardiac Electromechanics.* Frontiers in Physiology, 2018. **9**(1714).
8. Semciw, A.I., et al., *Gluteus medius: An intramuscular EMG investigation of anterior, middle and posterior segments during gait.* Journal of Electromyography and Kinesiology, 2013. **23**(4): p. 858-864.
9. Watanabe, K., M. Kouzaki, and T. Moritani, *Non-uniform surface electromyographic responses to change in joint angle within rectus femoris muscle.* Muscle & Nerve, 2014. **50**(5): p. 794-802.
10. Gottschalk, F., S. Kourosh, and B. Leveau, *The functional anatomy of tensor fasciae latae and gluteus medius and minimus.* Journal of anatomy, 1989. **166**: p. 179-189.
11. O'Sullivan, K., S.M. Smith, and D. Sainsbury, *Electromyographic analysis of the three subdivisions of gluteus medius during weight-bearing exercises.* BMC Sports Science, Medicine and Rehabilitation, 2010. **2**(1): p. 17.
12. Soderberg, G.L. and W.F. Dostal, *Electromyographic study of three parts of the gluteus medius muscle during functional activities.* Physical therapy, 1978. **58**(6): p. 691-696.
13. O’Dwyer, C., D. Sainsbury, and K. O’Sullivan, *Gluteus medius muscle activation during isometric muscle contractions.* Journal of Sport Rehabilitation, 2011. **20**(2): p. 174-186.
14. Kolk, S., et al., *Symmetry and spatial distribution of muscle glucose uptake in the lower limbs during walking measured using FDG-PET.* PLOS ONE, 2019. **14**(4): p. e0215276.
15. Goodwin, P.C., et al., *Reliability of leg muscle electromyography in vertical jumping.* European Journal of Applied Physiology and Occupational Physiology, 1999. **79**(4): p. 374-378.
16. Ghaderi, P. and H.R. Marateb, *Muscle activity map reconstruction from high density surface EMG signals with missing channels using image inpainting and surface reconstruction methods.* IEEE Transactions on Biomedical Engineering, 2017. **64**(7): p. 1513-1523.
17. Young, C.C., et al., *The effect of surface and internal electrodes on the gait of children with cerebral palsy, spastic diplegic type.* Journal of Orthopaedic Research, 1989. **7**(5): p. 732-737.
18. Barbosa, A.C., et al., *Increased activation amplitude levels of gluteus medius in women during isometric and dynamic conditions following a 4-week protocol of low-load eccentric exercises.* Physiotherapy Research International, 2016. **21**(4): p. 257-263.
19. Chen, Z., et al., *Effect of component mal-rotation on knee loading in total knee arthroplasty using multi-body dynamics modeling under a simulated walking gait.* Journal of Orthopaedic Research, 2015. **33**(9): p. 1287-1296.
20. Li, J., et al., *Unilateral total hip replacement patients with symptomatic leg length inequality have abnormal hip biomechanics during walking.* Clinical Biomechanics 2015. **30**(5): p. 513-519.
21. Webb, J.D., S.S. Blemker, and S.L. Delp, *3D finite element models of shoulder muscles for computing lines of actions and moment arms.* Computer Methods in Biomechanics and Biomedical Engineering, 2014. **17**(8): p. 829-837.

22. Zöllner, A.M., et al., *On high heels and short muscles: A multiscale model for sarcomere loss in the gastrocnemius muscle.* Journal of Theoretical Biology, 2015. **365**: p. 301-310.
23. Stelletta, J., R. Dumas, and Y. Lafon, *Modeling of the Thigh: A 3D Deformable Approach Considering Muscle Interactions*, in *Biomechanics of Living Organs*, Y. Payan and J. Ohayon, Editors. 2017, Academic Press: Oxford. p. 497-521.
24. Mo, F., et al., *A lower limb-pelvis finite element model with 3D active muscles.* Annals of Biomedical Engineering, 2018. **46**(1): p. 86-96.
25. Mo, F., et al., *Implementation of controlling strategy in a biomechanical lower limb model with active muscles for coupling multibody dynamics and finite element analysis.* Journal of Biomechanics, 2019. **91**: p. 51-60.
26. Li, J., et al., *Development of a finite element musculoskeletal model with the ability to predict contractions of three-dimensional muscles.* Journal of Biomechanics, 2019. **94**: p. 230-234.
27. Carbone, V., et al., *TLEM 2.0 – A comprehensive musculoskeletal geometry dataset for subject-specific modeling of lower extremity.* Journal of Biomechanics, 2015. **48**(5): p. 734-741.
28. Li, J., et al., *The influence of the representation of collagen fibre organisation on the cartilage contact mechanics of the hip joint.* Journal of Biomechanics, 2016. **49**(9): p. 1679-1685.
29. Weiss, J.A., B.N. Maker, and S. Govindjee, *Finite element implementation of incompressible, transversely isotropic hyperelasticity.* Computer Methods in Applied Mechanics and Engineering, 1996. **135**(1): p. 107-128.
30. Tsutsumi, M., A. Nimura, and K. Akita, *The gluteus medius tendon and its insertion sites: an anatomical study with possible implications for gluteus medius tears.* JBJS, 2019. **101**(2): p. 177-184.
31. Maas, S.A. and J.A. Weiss, *FEBio Theory Manual*. 2007: http://mrl.sci.utah.edu/software/febio.
32. Heintz, S. and E.M. Gutierrez-Farewik, *Static optimization of muscle forces during gait in comparison to EMG-to-force processing approach.* Gait and Posture, 2007. **26**(2): p. 279-288.
33. Adouni, M. and A. Shirazi-Adl, *Partitioning of knee joint internal forces in gait is dictated by the knee adduction angle and not by the knee adduction moment.* Journal of Biomechanics, 2014. **47**(7): p. 1696-1703.
34. Rasmussen, J., M. Damsgaard, and M. Voigt, *Muscle recruitment by the min/max criterion — a comparative numerical study.* Journal of Biomechanics, 2001. **34**(3): p. 409-415.
35. Dul, J., et al., *Muscular synergism—I. On criteria for load sharing between synergistic muscles.* Journal of Biomechanics, 1984. **17**(9): p. 663-673.
36. Li, J., et al., *Hip contact forces in asymptomatic total hip replacement patients differ from normal healthy individuals: Implications for preclinical testing.* Clinical Biomechanics 2014(0).
37. Gizzi, A., M. Vasta, and A. Pandolfi, *Modeling collagen recruitment in hyperelastic bio-material models with statistical distribution of the fiber orientation.* International Journal of Engineering Science, 2014. **78**: p. 48-60.
38. Vasta, M., A. Gizzi, and A. Pandolfi, *A spectral decomposition approach for the mechanical statistical characterization of distributed fiber-reinforced tissues.* International Journal of Non-Linear Mechanics, 2018. **106**: p. 258-265.
39. Röhrle, O., J.B. Davidson, and A.J. Pullan, *A physiologically based, multi-scale model of skeletal muscle structure and function.* Frontiers in physiology, 2012. **3**: p. 358-358.
40. Li, J., *Development and validation of a finite-element musculoskeletal model incorporating a deformable contact model of the hip joint during gait.* Journal of the Mechanical Behavior of Biomedical Materials, 2021. **113**: p. 104136.
41. Sinha, S., et al., *Muscle kinematics during isometric contraction: Development of phase contrast and spin tag techniques to study healthy and atrophied muscles.* Journal of Magnetic Resonance Imaging, 2004. **20**(6): p. 1008-1019.
42. Mazzoli, V., et al., *Accelerated 4D phase contrast MRI in skeletal muscle contraction.* Magnetic Resonance in Medicine, 2018. **80**(5): p. 1799-1811.
43. Blemker, S.S., P.M. Pinsky, and S.L. Delp, *A 3D model of muscle reveals the causes of nonuniform strains in the biceps brachii.* Journal of Biomechanics, 2005. **38**(4): p. 657-665.
44. Teran, J., et al., *Creating and simulating skeletal muscle from the visible human data set.* IEEE Transactions on Visualization and Computer Graphics, 2005. **11**(3): p. 317-328.

45. Röhrle, O. and A.J. Pullan, *Three-dimensional finite element modelling of muscle forces during mastication.* Journal of Biomechanics, 2007. **40**(15): p. 3363-3372.

Figure Legends

Fig. 1. a – FE model of the GM muscle in the original configuration (posterior-lateral view); b – fibre architecture in the tissue as illustrated by the blue arrows.

Fig. 2. GM models with subdivisions of varying dimensions in the original configuration (posterior-lateral view; anterior, medial and posterior subdivisions in blue, yellow and red, respectively; tendons in orange). a – GM subdivisions of similar dimension; b, c and d – one of the three GM subdivisions approximately 1.5 times larger than the other two portions.

Fig. 3. Contour of tensile stresses in the GM model in the original configuration (0 degrees rotation) and at 20 degrees rotation during abduction, internal rotation and external rotation (posterior-lateral view), showing stress distribution in GM under non-uniform contraction. The cost function was minimizing the sum of active contractile stresses cubed. The three subdivisions were of similar dimensions with boundaries marked by the black lines. Tensile stresses were concentrated around the tissue connecting the femur. Tensile stresses in all the subdivisions were of similar levels during hip abduction. Tensile stresses were markedly higher in the anterior subdivision and posterior subdivision during internal rotation and external rotation, respectively.

Fig. 4. Active contractile stresses in the GM subdivisions during abduction, internal rotation and external rotation. The three subdivisions were of similar dimensions. The cost function was minimizing the sum of active contractile stresses cubed. Active contractile stresses increased with increasing rotation angle during all the motions. All the subdivisions were activated during abduction, while only the anterior subdivision was activated during internal rotation. During external rotation, both the medial and posterior subdivisions were activated at 0 degrees and 5 degrees, while the medial subdivision became inactivated when the rotation exceeded 10 degrees. During abduction, active contractile stresses of the anterior and medial subdivisions were similar and higher than the posterior portion.

Fig. 5. Comparison of active contractile stresses during abduction calculated through different cost functions. The three subdivisions were of similar dimensions. The results were compared to the model with uniform contraction across the whole muscle (system not redundant and thus optimization not needed). Results of the models with uniform contraction and with the cost function of minimizing the maximum active contractile stress (min/max) were identical (the two curves overlap). There was a difference in the active contractile stresses under different cost functions, particularly in the posterior subdivision. A higher level of non-uniform contraction was observed under the cost function of minimizing the sum of active contractile stresses squared than minimizing the sum of active contractile stresses cubed. Under the two cost functions of minimizing the sum of active contractile stresses squared/cubed, active contractile stress increased with increasing abduction angle and was higher in the anterior and medial subdivisions than the posterior portion.

Fig. 6. Comparison of active contractile stresses during abduction in the GM with subdivisions of different dimensions. The cost function was minimizing the sum of active contractile stresses cubed. There was a marked difference in active contractile stresses among the models with subdivisions of different dimensions. The active contractile stress was higher in a larger subdivision compared with the same subdivision of the model with subdivisions of similar dimensions.

Fig 1

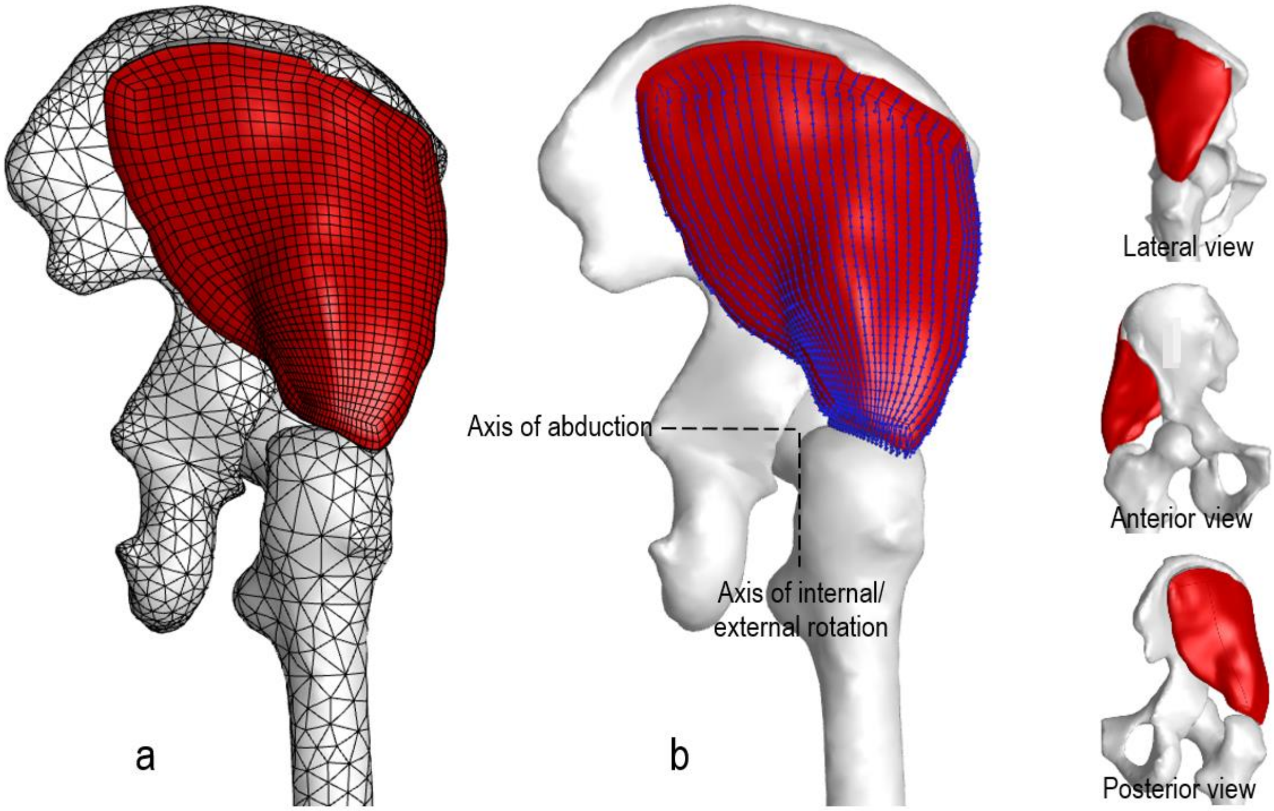

Lateral view
Axis of abduction
Anterior view
Axis of internal/
external rotation
Posterior view
a
b

Fig 2

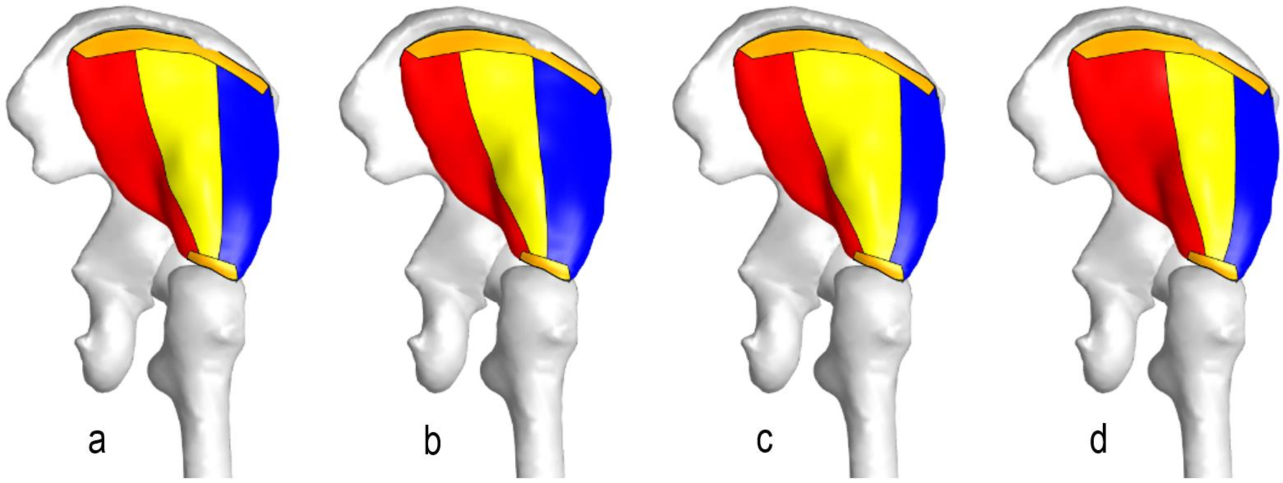

Subdivisions of similar dimensions

Larger anterior subdivision

Larger medial subdivision

Larger posterior subdivision

Fig 3

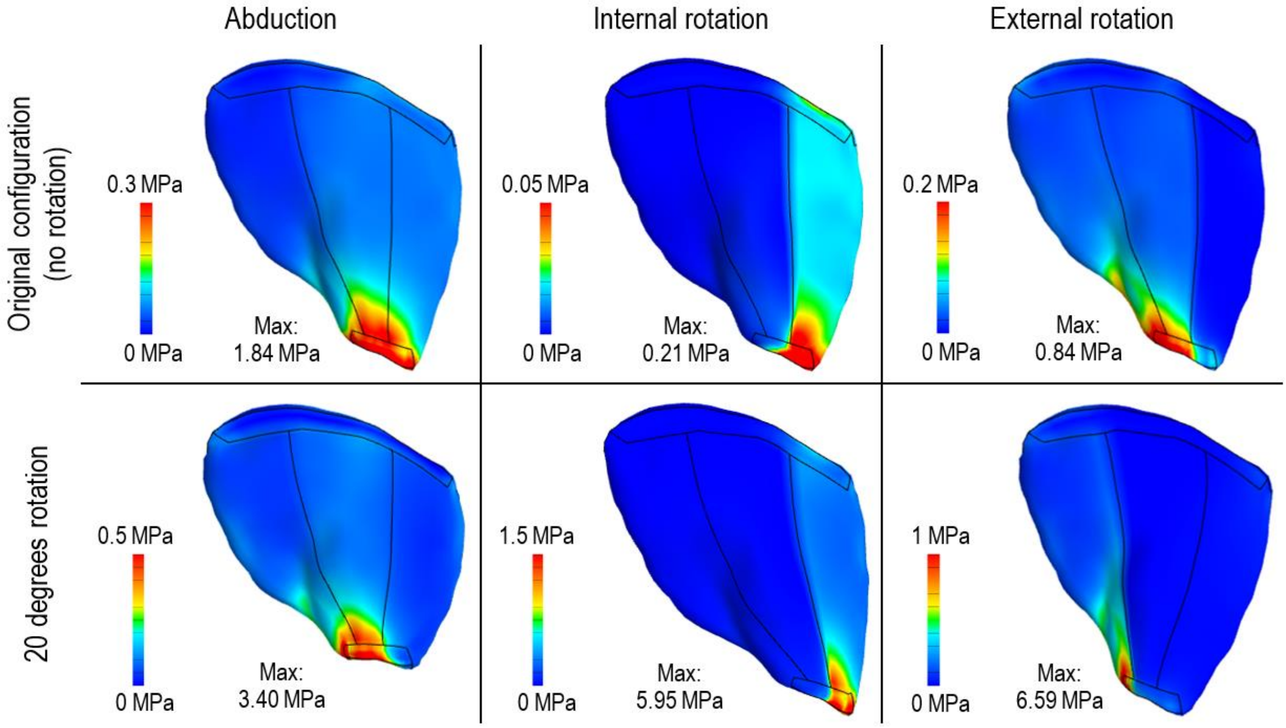

Abduction
Internal rotation
External rotation
Original configuration
(no rotation)
20 degrees rotation
0.3 MPa
0 MPa
Max:
1.84 MPa
0.05 MPa
0 MPa
Max:
0.21 MPa
0.2 MPa
0 MPa
Max:
0.84 MPa
0.5 MPa
0 MPa
Max:
3.40 MPa
1.5 MPa
0 MPa
Max:
5.95 MPa
1 MPa
0 MPa
Max:
6.59 MPa

Fig 4

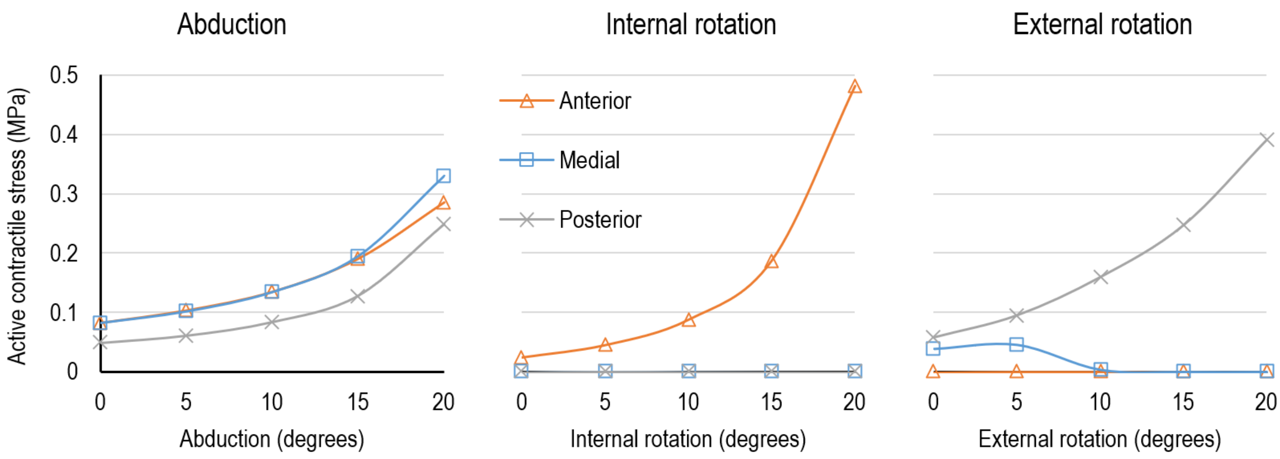

Abduction
Internal rotation
External rotation
Active contractile stress (MPa)
0.5
0.4
0.3
0.2
0.1
0
Anterior
Medial
Posterior
0 5 10 15 20
Abduction (degrees)
Internal rotation (degrees)
External rotation (degrees)

Fig 5

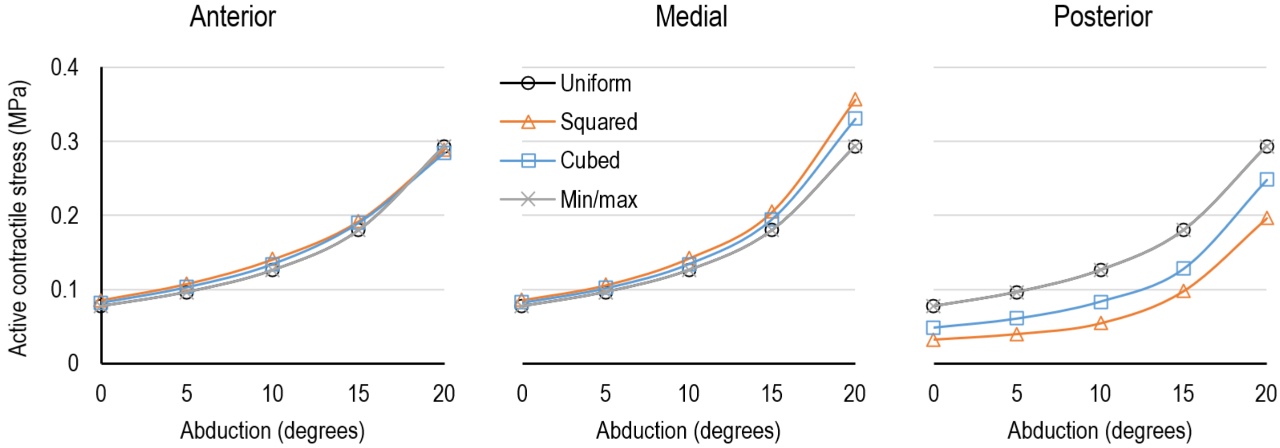

Anterior
Medial
Posterior
Active contractile stress (MPa)
0.4
0.3
0.2
0.1
0
0
5
10
15
20
Abduction (degrees)
Uniform
Squared
Cubed
Min/max

Fig 6

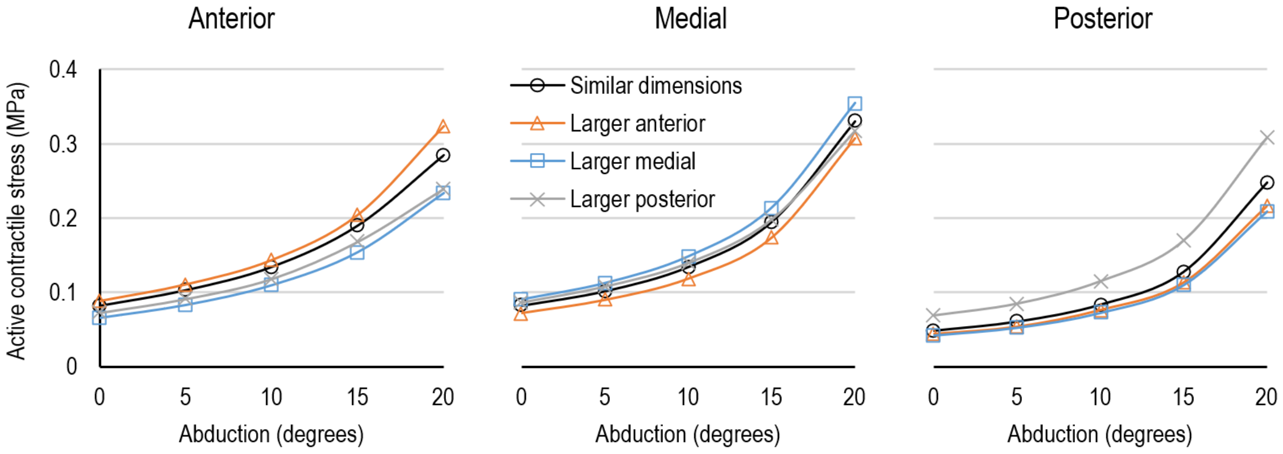

Anterior
Medial
Posterior
Active contractile stress (MPa)
0.4
0.3
0.2
0.1
0
0
5
10
15
20
Abduction (degrees)
Similar dimensions
Larger anterior
Larger medial
Larger posterior

List of Tables

Table 1. Constitutive model parameters. The values are based on previous studies [24, 43-45]. The maximum value of active contractile stress was 0.5 MPa.

Muscle constants		Tendon constants	
C_1	0.01 MPa	C_1	0.1 MPa
C_2	0.01 MPa	C_2	0.1 MPa
C_3	0.015 MPa	C_3	2.7 MPa
C_4	15	C_4	46.4
C_5	6 MPa	C_5	500 MPa
K	10 MPa	K	100 MPa
λ_m	1.4	λ_m	1.03